FATIGUE AND FRACTURE PARAMETER ESTIMATION OF A TURBINE BLADE

I.A. Ubulom
School of Engineering and Information Technology
University of New South Wales
Canberra, ACT, Australia

K. Shankar
School of Engineering and Information Technology
University of New South Wales
Canberra, ACT, Australia

A.J. Neely
School of Engineering and Information Technology
University of New South Wales
Canberra, ACT, Australia

ABSTRACT

This work presents a numerical estimation of fracture parameters for a turbine blade. A semi-elliptical crack of major and minor radii respectively of 0.5mm & 0.25mm was modeled on the turbine blade to investigate the influence of combined thermal, aerodynamic and cyclic loads on crack growth behavior. The aerodynamic and thermal loads were estimated from a compressible CFD code. The CFD code was validated by comparison against a publicly accessed experimental case.

The crack was modelled in the lower root region of the blade being a potential damage zone from effect of high cyclic stress and contacts with the disc attachment. Similarly, the alternating stresses obtained from the combined aerodynamic, thermal and cyclic loads were used to estimate the fatigue cycles.

NOMENCLATURE LIST

e	turbulent eddy dissipation
k	turbulent kinetic energy
K	stress Intensity factor
J	strain energy release
u_i	displacement vector
Γ	arbitrary crack volume
w	strain energy density
T_i	crack surface traction
ν	Poisson's ratio
σ_{th}	thermal stress
ds	crack contour increment
W_e	elastic strain energy density
R	stress ratio (K_{min}/K_{max})
K_{min}	minimum stress intensity factor
K_{max}	maximum stress intensity factor
SIFs	stress intensity factor
ε_{ij}	strain tensor
UTS	ultimate tensile strength
KIC	plane strain fracture toughness
α	thermal expansion coefficient
BEM	boundary element methods
FEM	finite element methods
CFD	computational fluid dynamics
RPM	revolutions per minute
SBL	shock boundary layer interaction
LCF	Low Cycle Fatigue
HCF	High Cycle Fatigue

INTRODUCTION

Fatigue failures in structural materials, most specifically on turbines, are recurrent issues and pose major challenges to operators and researchers. Despite the enormous volume of publication in this area, the problem still persists, but now with a deeper understanding from the early works of Wöhler [1].

In the high pressure section of gas turbines, fatigue failures arise given the adverse boundary conditions to which the blades are subject. To deliver the desired power and thrust needed for propulsion, the airfoils rotating at high RPM extract energy from the high pressure and temperature gas. The periodic operation of these components induces material failures in form of low-cycle and high-cycle fatigue, and in most severe cases, thermo-mechanical fatigue, [2] [3] [4]. As such, to ensure a reliable service delivery (and in-line with best practice) accurate predictions are necessary to avoid in-service failure which could lead to fatal consequences.

Two common approaches are used for fatigue failure estimation: a safe-life design, and the damage tolerant method. While both methods have inherent challenges, the suitability of the damage tolerant method to considering fatigue failures in two stages of crack initiation and propagation, makes it much more viable [5], [6]. The damage-tolerant process of fatigue analysis enables the estimation of fracture parameters, J-integral and stress intensity factors, which invariably characterize damage at the local microstructural level, [7] [8]. While the LCF modes are associated with plastic strain zones forming ahead of the crack-tips [7], the low amplitude HCF modes often lead to elastic range damages.

Previous studies have shown that significant economic gains could be achieved by the distinguishing the fatigue process into crack initiation and propagation cycles. By carefully scheduled inspection intervals, a crack of certain length could be monitored while the component is in service until a critical fracture length is reached. Much of these benefits

have been carefully discovered through myriads of experimental work. In light of this, [9] investigated fatigue crack growth for a wrought nickel-base alloy. The crack lengths were measured using a D.C potential drop technique on a double cantilever specimen for Nimonic 105 and IN 738 LC materials. Similarly, [10] presented a metallographic analysis of the fracture surface of turbine blade. They presented a detailed enlarged image of the fracture specimen with failure surface at the suction side near the area of the trailing edge. The sites of stress concentrations on the blade were clearly visible and regarded as possible areas of crack nucleation under varying cyclic stresses. Recently, [11] measured fatigue crack growth on compressor blades using a stroboscopic light microscope at resonance condition at frequencies in the range 500-800 Hz. The instance of blade failure was determined at the point when the blade's natural frequency dropped by 5%, equivalent to a crack size of 4-mm. A similar approach was given in [12].

One common challenge in the experimental works cited above is the level of uncertainty in their capability to measure crack tip parameters. Critical material behaviors, such as displacement histories in thick specimen geometry, are essentially inaccessible to most measuring techniques [13]. However, with numerical methods such as computational fracture mechanics, a complex material behavior can be properly simplified and discretized in a mesh-based algorithm from which solutions are readily obtained. With the recent advancements in computer processing speeds, complex problems can be readily studied on a parallel processing basis. Numerical computations enhance the adaptation of models of different materials, load histories and large-scale geometries. Such benefits make the approach a preferable method [12]. These advantages have led to considerable research interests in numerical modelling of fracture mechanics problems [14].

On turbine blade related fatigue problems, [15] presented a numerical evaluation of the fracture parameters for the failure investigation of a last stage steam turbine blade. Three key fracture areas were identified on the blades: a crack initiation site at a stress raiser point; a region of high damage impacts with initiation of fresh cracks propagating at a higher rate; and an area of unstable fracture. They examined the fatigue striations spacing for the three zones of fatigue at 0.1-0.3 μm and 8 and 12 μm respectively.

With the combined influence of thermal and mechanical loads, [16] reported a two-dimensional finite element problem formulation for the fracture analysis of the firtree region of the blade roots. Their study was undertaken for a crack size of approximately 1mm and 10.16mm being the assumed initiation and propagation lengths. The crack initiation process was attributed to the large thermal strains that occurred during the engine startup and shutdown period. A direct correlation was used to relate the stress intensity crack tip parameter as a function of the engine rotational speed. A similar study was performed by [17] who adopted a FEM approach to estimate the life of a turbine blade. The results were presented using the stress intensity factor as a suitable crack-tip parameter in the linear elastic fracture mechanics regime. [8] combined a strain life approach with fracture mechanics for a fatigue life evaluation of the high pressure turbine airfoils. They also investigated the dynamic stress response of the blade under varying crack defects. Recently, [18] investigated the vibration characteristics of a cracked turbine blade. The cracked faces were retained on the blades as virtual points in the reduced-order model. The presence of a surface crack defect was shown to alter the vibration response of a bladed disk, which led to some damage in the form of mode localization.

In this work however, the influence of combined aero-thermal and cyclic loads on crack growth behavior are investigated. The aerodynamic and thermal loads are predicted using a fluid solver. The obtained pressure and temperature fields are used as boundary conditions in the finite element code with an embedded semi-elliptical crack on the turbine blade. This therefore was used to investigate a semi-elliptical crack growth under a combined thermal, aerodynamic and cyclic load.

Both linear elastic and plastic zone crack tip parameters such as stress intensity factors and J-integral are computed. To address the problem of crack-tip singularity, an advanced crack mesh algorithm implicit in ANSYS was used for the semi-elliptical crack front meshing. By varying the circular mesh contours around the area integral of the crack front, mesh-independent solutions can be ensured. A special hybrid mesh was used at the fracture affected zone, while an efficient interpolation was done to overlay the tetrahedral mesh in the far field geometry boundary with the fracture affected area.

Similarly, the computed stress amplitude from the one-way coupled fluid-structure interaction simulation was used to estimate the fatigue cycle assuming a mode-1 crack failure type under tension. The fluctuating aerodynamic load amplitude was superimposed on the high magnitude cyclic stress for a frequency range of 1-hour flight time. With an initial surface crack length of 2mm, the Paris expression was used to estimate the propagation and fracture life of a specimen under varying amplitude loads, typical of that experienced by the high-pressure turbine blades. A similar approximation was used for the estimation of fatigue life of compressor blade [19]

Fluid Flow Model

A commercial finite volume code, ANSY CFX, was used to estimate the pressure and thermal loads of the Aachen turbine configuration. The model geometry was created following the flow conditions given in [20], [21]. Being a moderately

subsonic case, the effect of SBL was considered negligible. For the viscous flow case of the high-pressure turbine, the ideal gas material properties were specified in the fluid volume to accurately model the compressible gas behavior. A non-slip wall was maintained at the blade surface for which case the flow in the near wall region was restrained from penetrating the wall.

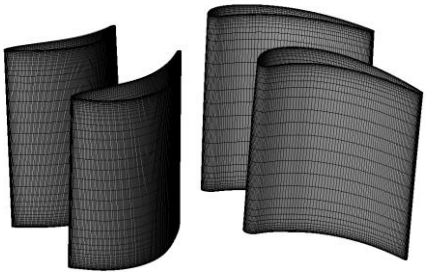

Figure 1: CFD surface mesh for stator and rotor Blades

For the heat transfer effect, the total energy option in the ANSYS CFX solver was used. This models the transport of enthalpy including the kinetic effects of the gas flow, and considered suitable for flows with Mach number > 0.3. A velocity outlet and inlet total pressure was specified from which the inlet static pressure was calculated by the solver. A nominal turbulence intensity of 5% was specified at the inlet in the absence of an experimentally determined value. This, however, is within the allowable turbulence intensity specification (0.1% - 10%) recommended for such cases, [22].

The standard k-e turbulence model was used to approximate the resolution of the turbulent fluctuations. This is a further modification of the eddy-viscosity model, which was earlier formulated to relate the flow Reynolds stresses to the local mean-velocity gradients. The standard k-e model uses a scalable wall-function approach to model near wall effects. The standard model implemented is also an improvement from the original k-e model which was limited by the numerous multiplicative variables in the closure terms for dissipation and kinetic energy transport. The modification was proposed by Launder and Spalding [23], in which the closure constants in the turbulent kinetic energy and dissipation energy transport equations were determined experimentally. This also enables its application for wall-bounded flows. Thus, the code is able to accept defined boundary conditions at the distance y^+_0 outside the viscous sublayer. The stability of the code was also enhanced by using the advance scheme to model the integration of the conservation equations through regions with large velocity gradients [24] [25].

Figure.1 shows the fluid surface mesh for the turbine stage blades, stator and rotor blades [L-R] with the direction of rotation into the page. A multi-block H-O-H grid code, Turbogrid, was used to generate the structured mesh. For effective near-wall modelling, the y^+ value was maintained at > 8, similar to that proposed in [22]. Given the likelihood of flow separation at the curved region of the leading edge, a fine grid was maintained at the blade stagnation regions of the leading edge with more than 100-grid nodes maintained in the stream-wise direction of the flow domain.

To model the required number of blades in the annulus, a rotational periodic boundary condition was maintained at the side walls of the flow domain.. A domain interface boundary enabled the connection of the outlet of the stator domain to the inlet of the rotor domain, through the general connection interface function in CFX. Noting the differences in the surface areas at the rotor-stator interface, a pitch change rotational offset angle of 10^0 and 8.78^0 were specified based on the sector number of the blades.

Finite element model

A 20-node solid element (SOLID227) was used to discretize the blade volume. The element is suitable for boundary value problems typical of fluid-thermal-structural interactions. The material's temperature dependent properties were specified in the finite element model, similar to that given in [26]

Since finite element formulation is highly mesh sensitive, further difficulties arise in having to precisely capture singular fields in the crack tip region. By defining the integration domain over a relatively large area, circular mesh contours were defined around the fracture affected zone with capability of mesh refinement at the crack tip region.

Figure 2 shows the discretization of the blade model with a modeled semi-elliptical crack as defined in the ANSYS FEA suite. This mesh method is robust given its capability to compute crack tip parameters even with relatively coarse mesh and hybrid capability for mesh refinement [27]. The region at which the crack was modelled was the region of highest maximum principal stress obtained from the previous FEA solutions reported in [28]

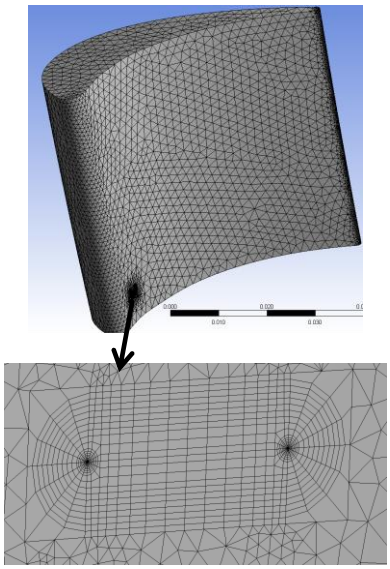

Figure 2 (a) Blade with embedded mesh

A local coordinate system was defined for the fracture-affected zone. The local crack area coordinate axis was defined as an offset from the global coordinate axis. The local X-axis in the fracture frame was defined in the direction pointing normal into the geometry surface while the local Y-axis points to the direction of crack tip front

J-Integral Formulation

The J-integral was originally proposed by [29] as appropriate crack-tip parameter in the elastic-plastic region. This is presented here in the form following that given in [30];

$$J = \int_{\Gamma} \left(w dy - T_i \frac{\partial u_i}{\partial x} ds \right)$$

Where Γ represents the arbitrary curve volume around the crack tip, w is defined as the strain energy density, u_i is the displacement vector component. The term T_i is the traction vector component, and ds is the increment along the contour for the local x and y coordinates. In the presence of thermal loads, [31] have shown that the computation of the J-line integral over a closed path does not necessarily meet the conditions of path-independence. They noted that by combining the J-integral with the area integral, the crack tip stress intensity factors could also be calculated for any path surrounding the crack tip. Thus, by computing the J-integral from an area integral of the crack path, an accurate approximation was obtained compared to that obtained via the conventional displacement interpolation method. The method adopted in this work however is similar to that proposed by [32] [33], where a divergence theorem is used to expand the J- contour integral over the volume of the fracture affected zone of the 3-D blade. The mathematical derivation of this approach was given in [34] [33].

To incorporate the 3-D thermal effect characterized by significant plasticity and large-scale yielding, the mathematical formulation similar to that given by [35] was followed. The energy change in the fracture zone per unit crack length, $E_{f,}$ was given by;

$$E_f = \int_{A_f} T_i \frac{\partial u_i}{\partial x_i} \partial A \qquad (i = 1,2,3)$$

This was related to the energy integral term, J_k, defined per unit crack length at a point in the orthogonal crack coordinate x_i, as;

$$J_k = -{}^{1}/_{L_t} \int_{A_f} \Re \partial A \qquad (i = 1,2,3)$$

Thus, A_f is the fracture affected area, and $\Re = T_i \frac{\partial u_i}{\partial x_i}$. The variable L_t is the total crack length, and T_i is the traction acting on the surface while u_i is the displacement in the i_{th}-direction. The energy release rate per unit crack length, $J_{k,}$ therefore was expressed in a form devoid of dependence on singular stress-strain term as;

$$J_k = -\frac{1}{L_t} \left[\int_{A+A_s} \Re \partial A - \int_{v} E \partial v \right] \quad (i,j,k = 1,2,3)$$

And with thermal stress effect as ;

$$J_k = \frac{1}{L_t} \left[\int_{v} \frac{\partial W_e}{\partial X_k} \partial v - \int_{A+A_s} \Re \partial A + \int_{v} \sigma_{ij} \frac{\partial \mathcal{E}_t}{\partial X_k} \partial V \right]$$

$$(i,j,k = 1,2,3)$$

where $E = \sigma_{ij} \frac{\partial \mathcal{E}_{ij}}{\partial X_k}$, and σ_{ij} is the stress tensor. The strain tensor $\mathcal{E}_{ij}$ was defined in terms of the elastic and thermal strains. The thermal strain $\mathcal{E}_t = \alpha \delta_{ij} \Delta T$. Where v is the volume of the area enclosed by the crack. The terms A, A_s are the total area of the crack sliced body and crack surface area respectively. The term δ_{ij} is the Kronecker delta and α is the thermal expansion coefficient. ΔT is the temperature variation while W_e is the elastic strain energy density. A more detailed formulation of the above can be found; [36], [37] [38].

To simulate the growth phenomenon, the ANSYS suite uses the Gurson's model, which is better suited for a progressively damaged material under external loading. The model uses a micromechanic-based parameter to represent the ductile process of void growth and nucleation, [39].

The stress intensity factor assuming a first fracture failure mode was computed from a correlation with the J-integral term. For a plane stress and plain strain loading, the SIF can be estimated using the expressions;

$$J = {}^{1}/_{E_T} K_I^2 \quad \text{Plane stress}$$

$$J = \frac{(1-v^2)}{E_T} K_I^2 \quad \text{Plane strain}$$

Where E_T is the material's modulus defined as a function of temperature. For a typical turbine blade material, [40] noted that at low ΔK, the failure cycles will operate mainly under plane strain fracture during growth. On the other hand, at high ΔK, an indication of the plane stress fracture is the formation of shear lips across the failure surface. While a smaller plastic zone size is usually associated with plane strain, the larger plastic zone in the plane stress condition increases the amount of crack growth retardation. This is due mainly to the fact that high levels of residual plasticity associated with plane stress regions cause more asperities to be brought in contact between the upper and lower surface of the failure plane. A plane strain condition is therefore assumed in this work similar to that in [41]. They noted that at the crack tip of the turbine blade, the low ductility nature of the blade material causes low deformation during a crack propagation phase.

Thus a semi-elliptical crack of major and minor radii 0.5mm and 0.25mm respectively was modelled in the high stress lower region of the blade. A cyclic rotational velocity was applied as an FE boundary condition, alongside superimposed thermal and pressure loads from a steady CFD solutions. Three temperature cases of 370K, 630K and 1130K were modelled at which points there are significant effects of temperature on the material yield strength.

For the crack area meshing, a hybrid structured mesh was defined around the major and minor crack axes. A cylindrical coordinate was created at the crack area with the crack x-axis directed into the geometry surface while the y-axis points in the direction of crack propagation. The solver uses an interpolation approach to connect the crack-tip mesh to the SOLID227 tetrahedral mesh used in the far field body. A mesh refinement study on the crack area was performed by varying three crack mesh properties including; contour radius, circumferential crack division and the mesh contours, see [39]. A mesh-independent solution was obtained by observing the variation of the J-integral values along the crack front. This is shown in Figure 7.

Crack Growth and Fatigue Estimation under Transient Turbine load history

For the fatigue cycles analysis, LCF and HCF load amplitude were obtained from the fluid-flow solution and cyclic rotational stress in the FEA domain respectively. The load history was decomposed in a form typical of engine flight spectrum shown in figure 3. The HCF fluctuations due to the aerodynamic loads were superimposed on the LCF load from a 0-8000 RPM constant speed operation. A similar approximation was reported in [19] who investigated LCF-HCF interaction for compressor blade geometry.

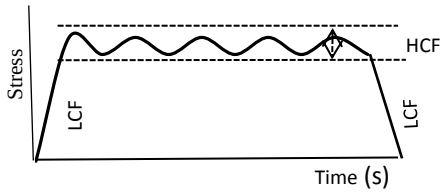

Figure 3: Typical engine flight spectrum

The decomposed load history was used to investigate the behavior of a geometry under varying amplitude load similar to that experienced by a turbine blade. The crack specimen width, w, was specified as 50mm. This was to represent a crack growth in the direction across the chord length of the blade, see [42]. The blade material modelled was a quenched and tempered structural steel HY-80 with yield strength of 617 MPa. The plain strain fracture toughness for this case was 146 (MPa ($m^{1/2}$)) [43]. The rest of the material's fracture parameters including the Paris law coefficient and exponent are similar to those reported in [42]. Given all materials are assumed to contain a crack, an initial edge crack of 2mm was modelled while the final crack length was that determined by the material's fracture toughness.

RESULTS

The results for the steady CFD fluid solution are shown in figures 4 and 5. The case of the transient load history for this test case was reported in previous work of the authors in [41]. Figure 4 shows the contour plots for the pressure and Mach number distributions respectively. Also shown in Figure 5 are the coefficient of pressure comparison against experimental data of [20] [21] for the stator blade, at three different span positions. Being a purely subsonic case, less shock wave effect was noticed. While the predictions show strong three dimensional flow features, the flow across the suction side of the blade was fully attached. The predictions for the rotor blade geometry were reported in [28]

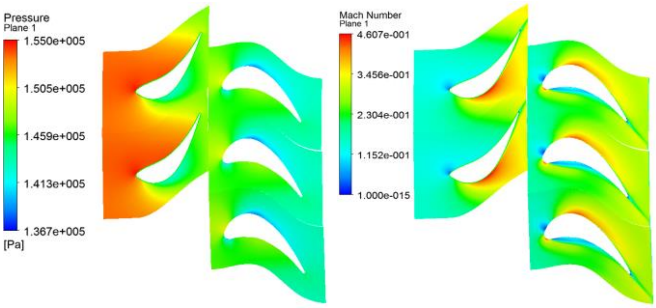

Figure 4: Pressure and Mach number contours

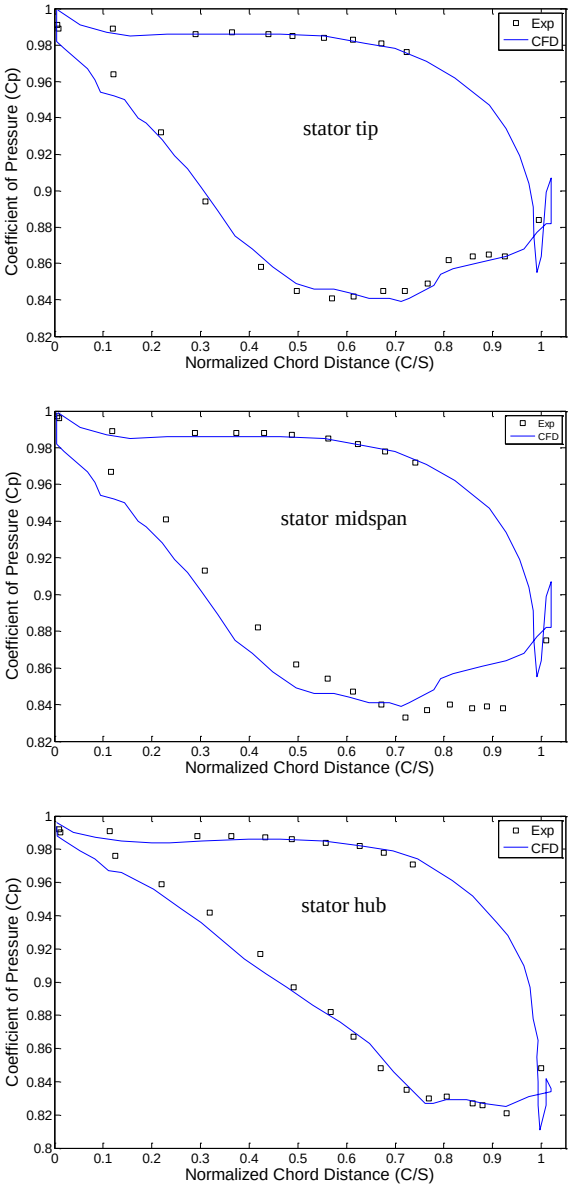

Figure 5: Coefficient of pressure comparison against experimental data [19-20]

From the coefficient of pressure plot in figure 5, a region of pressure stability was noticed on the upper surface. This was shown by the relatively constant pressure coefficient maintained immediately after the leading edge 20% chord position to about 70% downstream, after which the flow accelerates towards the trailing edge. On the suction surface, the accelerating flow remained fully attached on the surface until the 80% chord position at which point the flow speed begins to reduce leading to some adverse pressure effects close to the trailing edge. Overall, the fluid flow predictions show a reasonably close match with the experimental data. A more detailed description of the three-dimensional flow features of this geometry was reported in [20] [43].

Figure 6 shows the surface pressure and temperature obtained from the CFD solutions. These were transferred to the finite element model as boundary conditions with an embedded semi-elliptical crack on the blade geometry.

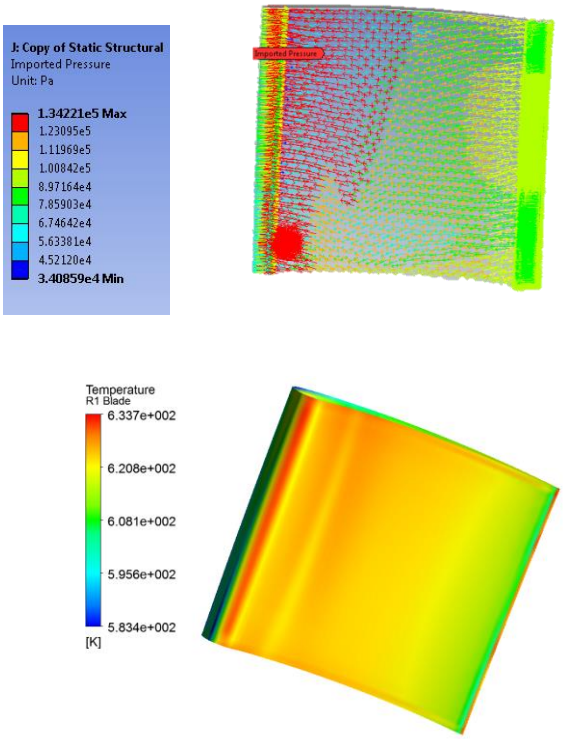

Figure 6: Imported pressure and temperature loads

Three different ranges of upstream flow temperatures, 370K, 630K and 1170K, were solved to determine the resulting non-uniform temperature on the blade surface. Each of these conditions was imported alongside a constant flow domain pressure of 155-kPa maintained at the stator inflow boundary. By using these conditions as initial boundary conditions in the finite element solver, a non-uniform thermal wall condition was formulated to investigate the effect of

temperature induced stress on crack-tip stress parameters, intensity factor and J-integral.

From the mesh sensitivity study, an optimum mesh level was obtained by observing that the J-integral crack tip parameter for each refinement does not differ by more than 1 J/m$^{2.}$ This is shown in plot figure 7, the normalized stress on the ordinate axis being the ratio of the materials modulus to the computed equivalent Von Mises stress. While the evaluation of equivalent stress in the far-field geometry was sensitive to local mesh refinements, the computation of the J-integral component was less sensitive. This is due to the fact that its related parameters were estimated based on the global energy release rate in the equivalent domain method. As noted by [44], the J-integral defines the closed contour integral of the strain energy density and the work done by traction acting on the crack tip. The crack-tip condition is determined based on the rate of change of total potential energy with respect to the crack length.

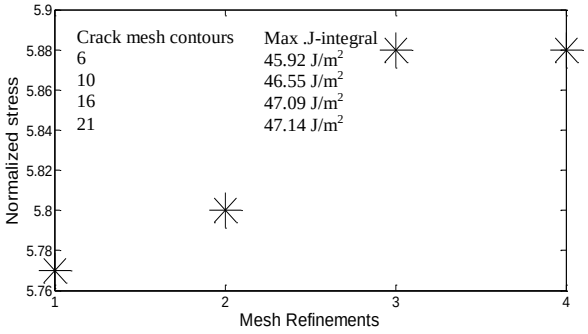

Figure 7: mesh refinement study

J-integral Computation under Combined Thermal, Aerodynamic and Cyclic Loads

Figure 8 shows the computation of the J-integral over the crack tip fronts for an applied static load for a rotational speed of 8000-rpm. This was shown for a temperature case of 370K alongside the pressure loads from figure 6. The total deformation and stress contour plot for this load case is shown in Figure 9. The maximum equivalent von Mises stress obtained from the superposition of these loads was approximately 511MPa. The spanwise distribution of the maximum deformation is shown with maximum value, 0.08mm computed at the blade tip position. The model is constrained from displacement in the three coordinate axes at lower root region. A parametric language subroutine was inserted to allow rotational and temperature effects for the estimation of thermal-mechanical stress

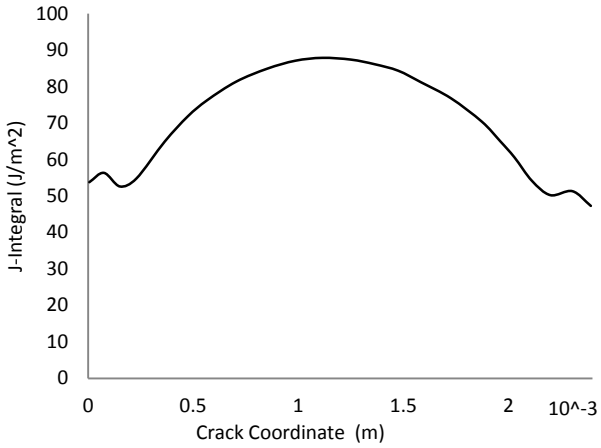

Figure 8: J-integral Computation at 370K Max. non uniform temperature

The maximum aerodynamic pressure of 134 kPa, computed from the CFD analyses was superimposed alongside the static centrifugal load. As shown, the J-integral increased steadily across the crack front with a maximum noticeable at the crack front 1.2mm. This being the region of maximum energy release per unit crack area. The distribution shows a symmetric pattern across the two ends of the crack front, with the highest point in the mid region of the fracture-affected area. A similar distribution of J-integral computation for a compressor blade was reported in [45].

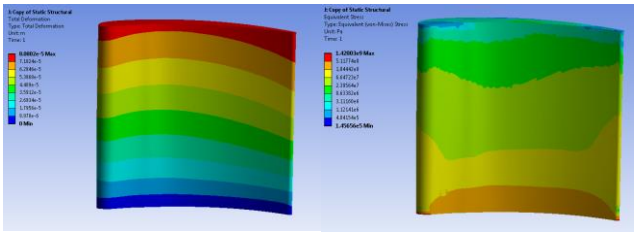

Figure 9: Total deformation and equivalent von Mises plot

Figure 10 shows the stress intensity factor computation along the crack front for various thermal stress loads. With an initial temperature value 370K, three cases were examined with a maximum value of 1130K. Each of the cases were analyzed alongside imposed aerodynamic and cyclic loads. The plot shows an increase in the magnitude of the stress intensity factor range from 4.76 MPa$\sqrt{m}$ to 7.88 MPa$\sqrt{m}$. For the third condition with maximum temperature of 1130K, the stress intensity factor increases to approximately 14.3 MPa$\sqrt{m}$. The computed curve of the SIF computation is similar to that of J-integral with symmetric condition at the deepest point on the crack, at crack length position 1.2mm.

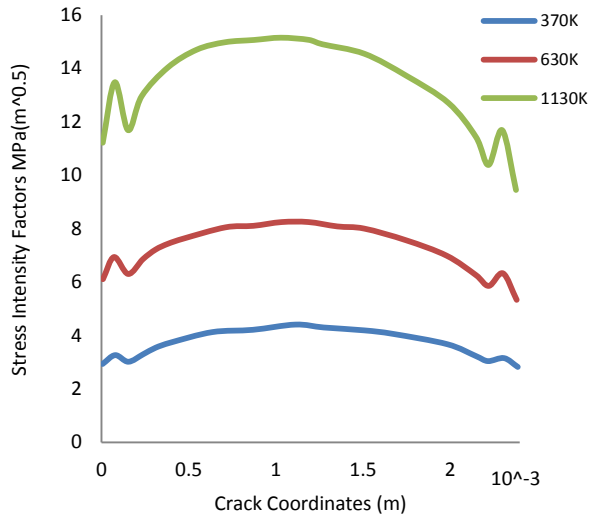

Figure 10: Stress intensity computations for varying non-uniform temperature

For temperatures as high as 1170K, the material behavior would be strongly characterized by the generation of motion and dislocation of grain boundaries. Thus, the fatigue process will be controlled by diffusion and corrosion processes as described in [7]. They noted that for a material of turbine blade configuration, at high temperature, material properties change from a ductile transgranular to a quasi-brittle integranular at above 550^0C from which an onset of thermal fatigue failure is likely imminent. [3] described crack initiation and propagation at elevated temperatures on turbine materials to be characterized by three phases of crystallographic cracking along the slip planes, transgranular and intergranular cracking occurring along the normal direction of the applied stress. The computation in figure 10 however is for mode I fracture for which the material experiences blunting and crack tip sharpening. A decrease in the SIFs for all the temperature range examined at the crack length 0.18mm position could be attributed to a combined influence of compressive stresses induced by the thermal loads at the end points of the fracture affected zone.

Alongside the decreasing yield strength from the high temperature, a sizeable plastic wake forms at the crack tip location. [46] investigated the effect of temperature on crack tip parameters and presented a direct correlation between high temperature effects and the size of the plastic wake zone. Recently, [47] noted that these increased plasticity is more likely at the component surface due to plane stress effect which acts to redistribute the local stresses. Figure 11 shows the stresses with evolving plastic wake due to the combined thermal, cyclic and aerodynamic loads modelled in this case.

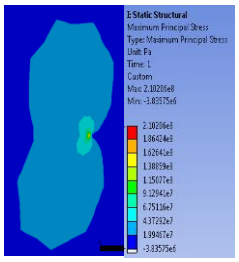

Figure 11: Stress contours in the crack affected region

A total of 12-circular mesh contours were modelled for the semi-elliptical crack radius. It should be noted that while the stress value obtained on the contour closest to the crack tip was relatively high, the solution is independent of stress singularity since the maximum stress region on the crack affected area is not on the crack tip location. A similar prediction was obtained in the work by [17] who investigated a turbine blade crack growth in a corrosive environment.

Crack Growth and Fatigue Cycles Estimation

The fatigue life estimation using the strain based approach for this configuration was reported in [28]. The LCF stress amplitude was estimated as 290MPa while the HCF fluctuation amplitude was 15MPa. The load history was formulated by superimposing the HCF fluctuations on the LCF following a typical turbine load pattern of figure 3. This was done for an estimated load cycle of 1-flight hour used to represent the takeoff and cruise and landing phase.

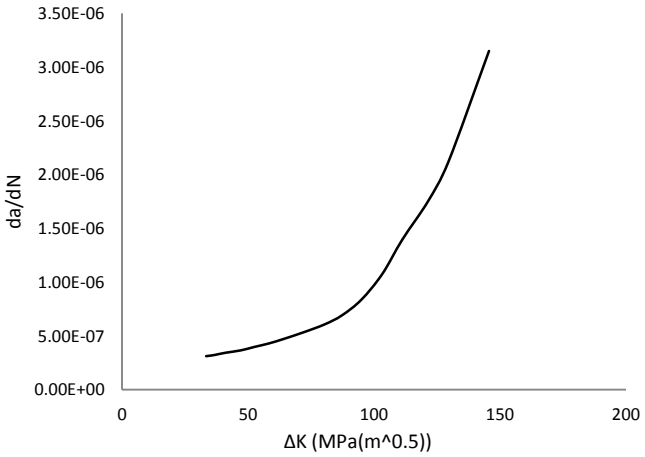

Figure 12: crack growth rate vs SIF range

Figure 12 shows the estimated crack growth rate versus the stress intensity factors. For this case, the component was assumed to have an inherent crack of size 0.002m. The final fracture was obtained at 18mm of crack length after which

the estimated stress intensity factor exceeded the material fracture toughness of 136 MPa ($m^{1/2}$).

At the lower growth regions, the material behavior is largely influenced by material microstructural composition. Thus, the local material inhomogeneity controls the material's resistance to crack propagation. At the high growth rate regions (da/dN ~ 10-6mm/cycles) the material's fracture resistance changes as the value approaches the fracture toughness, K_{IC} [48].

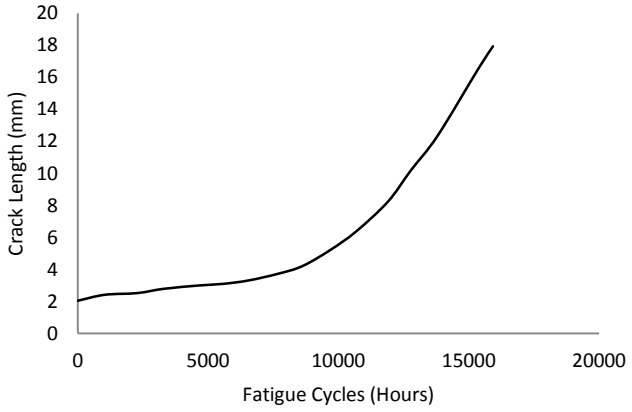

Figure 13: Crack length vs fatigue cycles [hours]

Figure 13 shows the estimated fatigue life of the CT specimen under a turbine blade loading history. The final crack length of 18mm was estimated as the critical crack length. This was modeled for a specimen width equivalent to the chord length of the turbine geometry, 50mm. For this material, steel HY-180, the Paris constant, C=3.43E-09, and the exponent, m=1.38.

While the prediction shows life estimation based on LCF-HCF loads superimposition, a simple analysis was performed to quantify the effects of the HCF loads amplitude on the overall fatigue life although not shown here for conciseness. At the low stress range of 15MPa, it was noticed that the crack would rarely propagate significantly through the geometry, given that the material exhibits high fracture toughness. However, it should be stated that with load frequency effects, the life would be much more reduced due to the HCF effects. By increasing the HCF stress amplitude by a factor of 3, an equivalent crack length of 18-mm was obtained at 8.5E5 hour cycles. Thus, without accounting for the frequency of loading, the LCF load range was shown to be the more damaging case for this test condition.

CONCLUSION

This work presented the computation of crack-tip parameters, J-integral and stress intensity factors for the turbine blade under combined influence of thermal, aerodynamic and cyclic loads. Three temperature cases were computed showing a corresponding increase in SIF with temperature loadings. Similarly, the computed stresses were used to estimate the fatigue crack propagation cycles of the blade.

While this analysis assumes an initial surface crack, it should be noted that the turbine component is susceptible to a more complex time-dependent flaw growth. This is complicated by the combined effect of corrosive environment and creep damages on the flaw growth pattern. In order to estimate and quantify a realistic inspection interval for its extended life, meaningful data will be required from real service load histories and in-situ material properties. A reasonable economic benefit could be achieved where inputs from nondestructive evaluations could be used to inform the scheduling of inspection interval periods.

ACKNOWLEDGMENTS

The authors wish to extend their appreciation to Total E & P Nig. Ltd, Port Harcourt for their support in this work. Computing support was provided from the NCI National Facility systems through the National Computational Merit Allocation Scheme supported by the Australian Government.

REFERENCES

[1] Wohler A., "Uber die Festigkeitis-Versuche mit Eisen und Stahl," *Zeitschrift fur Bauwesen*, vol. 20, no. 73, 1870.

[2] North Atlantic Treaty Organization (NATO), "Thermal Mechanical Fatigue of Aircraft Engine Materials," in *Advisory Group for Aerospace Research and Development*, Banff, Canada, 1996.

[3] D.A. Wilson, D.P.Deluca and B.A.Cowles, "Fatigue Crack Growth Resistance of Advanced Blade Material," in *Transactions of the ASME Turbo Expo - 86-GT-253*, Dusseldorf, 1986.

[4] J.Bressers, A Bennett, E.E.Affeldt and J.M.Martinez-Esnaola, "Thermomechanical Fatigue cracks in Coated and Uncoated Turbine Materials," A Publication of Joint Research Center, EC-Petten, Project ID: BE-0338, Netherlands.

[5] Vladimir V. Bolotin, Mechanics of Fatigue, Florida: CRC Press, 1999.

[6] Vasilios Zitounis, "Fatigue Crack growth Under variable Amplitude load Spectra Containing tensile loads," PhD Thesis of Cranfield University, Dept. of Industrial and Manufacturing Science, Bedford, UK, 2004.

[7] Ulrich Krupp, fatigue Crack Propagation in Metals and Alloys, Weinham: Wiley-VCH Verlag GmbH & Co. KGaA, 2007.

[8] N.S.Vyas and Sidarth and J.S.Rao, "A Fracture Mechanics Approach to Life Predictions of Turbine Blades- 93-GT-406," in *International Gas Turbine and Aeroengine Congress and Exhibition*, Ohio, 1993.

[9] R.B.Scarlin, "Creep and Fatigue Crack Growth in Overaged Nickel-base Alloys," *Materials Science and Engineering*, vol. 30, pp. 55-64, 1977.

[10] S,Qu*, C.M.Fu, C.Dong, J.F.Tian and Z.F.Zhang, "Failure Analysis of the 1st Stage Blades in Gas Turbine Engine," *Engineering Failure Analysis*, vol. 32, pp. 292-303, 2013.

[11] V.T.Troshchenko and A.V.Prokopenko, "Fatigue Strength of Gas Turbine Compressor Blades," *Engineering Failure Analysis*, vol. 7, pp. 209-220, 2000.

[12] Dong Woo Lee, Seok Swoo Cho, Soon Hyeok and Won Sik Joo, "Failure Analysis of Turbine Blade in atomic Power Plant," *Journal of Mechanical Science and Technology*, vol. 22, pp. 864-870, 2008.

[13] R.C.McClung and H.Sehitoglu, "On the Finite Element Analysis of Fatigue Crack Closure; Basic Modelling Issues," *Engineering Fracture Mechanics*, vol. 33, pp. 237-252, 1989.

[14] Meinhard Kuna, Finite Elements in Fracture Mechanics: Theory-Numerics-Applications. (Solid Mechanics and its Applications. Vol.201), Germany: Springer, 2013.

[15] N.S.Vyas, Sidarth and J.S.Rao, "Dyanmic Stress Analysis and a Fracture Mechanics Approach to Life Prediction of Turbine Blades," *Journal of Mechanics and Machine theory*, vol. 32, no. 4, pp. 511-527, 1997.

[16] A. A. Aziz, "Assessment of Crack Growth in a Space Shuttle Main Engine of First Stage High Pressure Fuel Turbopump Blade," *Journal of Finite Element Analysis and Design*, vol. 39, pp. 1-15, 2002.

[17] C.Cuevas Arteaga, J.A.Rodriquez, C.M.Clemente, J.A.Sequra, G.Urguiza and Y.El.Hamzaoui, "Estimation of Useful Life in Turbine Blades with cracks in Corrosive Environment," *Engineering Failure Analysis*, vol. 35, pp. 576-589, 2013.

[18] Akira Saito, Mathew P.Castenier and Christophe Pierre, "Effects of Cracked Blade on Mistuned Turbine Blade Engine Rotor Vibration," *Journal of Vibration and Accoustic*, Vols. 131-061006, pp. 1-9, Undated.

[19] Priyanka Dhopade, "Aeromechanical Modelling of Rotating Fan Blades to Investigate High-Cylce and Low Cycle Fatigue Interaction," PhD Thesis of University of New South Wales, Canberra, Australia, 2013.

[20] H. Gallus, K. Weskamp and J. Zeschky, "Computational Predictions and Measurements of the Axial Flow Turbine Cascade and Stages," in *Secondary Flows in Turbomachines*, Luxembourg, AGARD Conference Proceedings No.469, 1990, p. Chapter 21.

[21] H. Gallus, J. Zeschky and C. Hah, "Endwall and Unsteady Flow Phenomena in an Axial Turbine Stage," *39th International Gas Turbine and Aeroengine Congress and Exhibition*, pp. 94-GT-143, 1994.

[22] ANSYS. Inc, "ANSYS CFX-Solver Theory Guide," ANSYS.Inc Southpointe, 275 Technology Drive Canonsburg, 2009.

[23] Spalding D.B, "A Novel Finite Difference Formulation for Differential Equations Involving both First and Second Derivatives," *International Journal of Numerical Methods in Engineering*, vol. 4, pp. 551-559, 1972.

[24] Tuncer Cebeci, Analysis of Turbulent Flows (Second Revised and Expanded Edition), Oxford, UK: Elsevier Ltd, 2004.

[25] T.J Chung, Computational Fluid Dynamics (Second Edition), New York: Cambridge University Press, 2010.

[26] J.S.Rao, "Application of Fracture Mechanics in the Failure Analysis of a Last Stage Steam Turbine Blade," A Publication of Mechanical Engineering Department, Indian Institute of TEchnology,pp 599-610, New Delhi, India, 1997.

[27] W. Brocks and I. Scheider, "Numerical Aspect of the Path-Dependence of the J-integral in Incremental Plasticity," A Technical Note GKSS/WMS/01/08, 2001.

[28] I.A.Ubulom, K.Shankar and A.J.Neely, "Turbine Blade Life Prediction using Fluid-thermal-Structural Interaction Modelling, GT2015-43071," in *Proceedings of ASME Turbo Expo: Turbine Technical Conference and Exposition*, Montreal, Canada, 2015.

[29] Rice J.R., "A Path Independent Integral and the Approximate Analysis of Strain Concentration by Notches and Cracks," *Journal of Applied Mechanics*, vol. 35, pp. 379-386, 1968.

[30] Xian-Kui Zhu and James A Joyce, "Review of Fracture Toughness (G,K,J,CTOD,CTOA) Testing and Standardization," *Engineering Fracture Mechanics*, vol. 85, pp. 1-46, 2012.

[31] W.K.Wilson and I.W. Yu, "The use of the J-integral in Thermal Stress Crack Problems," *International Journal of Fracture* , vol. 15, no. 4, pp. 377-387, 1979.

[32] G.C.Shih and B.M. Barthelemy, "Mixed Mode Fatigue crack growth Predictions," *Journal of Engineering Fracture Mechanics*, vol. 13, pp. 439-451, 1980.

[33] G.P.Nikishkov and S.N.Atluri, "Calculation of Fracture Mechanics Parameters for an Arbitrary Three-Dimensional Crack, By the "Equivalent Domain Integral' Method," *Internation Journal for Numerical Methods in Engineering*, vol. 24, pp. 1801-1821, 1987.

[34] G.P.Nikishkov and S.N.Atluri, "Three-Dimensional

Elastic-Plastic J-Integral Calculations for Semi-Elliptical Surface Cracks in a Tensile Plate," *Engineering Fracture Mechanics,* vol. Vol.29, no. 0013-7944, pp. 81-87, 1998.

[35] Wen-Hwa Chen and Chin-Cheng Huang, "Analysis of Three-Dimensional Thermoelastic Fracture Problems using Path-Independent Integrals," *Engineering Fracture Mechanics,* vol. 39, no. 3, pp. 581-589, 1991.

[36] D.N.dell' Erba and M.H.Aliabadi, "BEM analysis of fracture problems in three-dmiensional thermoelasticity using J-integral," *International Journal of Solids and Structures* , vol. 38, pp. 4609-4630, (2001).

[37] N.N.Prasad, M.H.Aliabadi and D.P.Rooke, "Thermomechanical Fatigue Crack Growth," *International Journal of fatigue,* vol. 18, no. 6, pp. 349-361, 1996.

[38] G.P Nikishkov and S. N. Atluri, "An Equivalent Domain Integral Method for Computing Crack-Tip Integral Parameters in Non-Elastic, Thermo-Mechanical Fracture," *Engineering Fracture Mechanics,* vol. 26, no. 6, pp. 851-867, 1987.

[39] ANSYS Inc. Southpointe, "Structural Analysis Guide," ANSYS, Canonsburg, 2009.

[40] Vincent Mark Barker, "Thermomechanical Fatigue Crack Growth Modelling of a Nickel-base Superalloy," M.Sc. Thesis of Geogia Institute of Technology, USA, 2011.

[41] W.P.Foo and R.Castillo, "Fracture Mechanics Approach to Creep Growth in Welded IN739LC Turbine Blades.," in *International Gas Turbine and Aerospace Congress Exhibition*, Orlando, Florida, 1991.

[42] nCode DesignLife, "GlyphWorks Worked Examples," HBM Technical Support Document, UK, 2012.

[43] I.A.Ubulom, A.J.Neely and K.Shankar, "Heat Transfer Prediction of a Turbine Stage using Fluid-Thermal-Structural Interaction Simulation," in *19th Australian Fluid Mechanics Conference*, Melbourne, Australia, 2014.

[44] I.S.Raju and K.N.Shivakumar, "Implementation of Equivalent Domain Integral Method in the Two-Dimensional Analysis of Mized Mode Problems," *Analytical Services and Materials, Inc.,* Undated.

[45] Kirthan L.J, Ramakrishna Hedge, Suresh B.S and Girish Kumar.R, "Computational Analysis of Fatigue Crack Growth Based on Stress Intensity Factor Approach in Axial Flow Compressor Blades," *Procedia Materials Science,* vol. 5, pp. 387-397, 2014.

[46] Jong-Hoon Lee, Bum-Joon Kim, Moon Ki Kim and Byeong-Soo Lim, "Effects of Temperature and Oxidation on Threshold stress Intensity Factor of 12% Cr Steel for Steam Turbine Rotor Component," *Journal of Mechanical Science and Technology,* vol. 27 (5), pp. 1273-1277, 2013.

[47] N.B.McFayden, R.Bell and O.Vosikovsky, "Fatigue Crack Growth of Semi-Elliptical Surface Cracks," *International Journal of Fatigue,* vol. 12, no. 1, pp. 43-50, 1990.

[48] R.O.Ritchie, "Near-Threshold Fatigue Crack Propagation in Steels," *Publication of Metal Reviews,* no. 5 & 6, pp. 205-230, 1979.

[49] M.Gosz, J.Dolbow and B.Moran, "Domain Integral Formulation for Stress Intensity Factor Computation along Curved Three-Dimensional Interface Cracks," *International Journal of Solids and Structures,* vol. 35, no. 15, pp. 1763-1783, 1998.

[50] Ani Ural, Paul A Wawrzynek and Anthony R.Ingraffea, "Simulating Fatigue Crack Growth in Spiral Bevel Pinion," Publication of the NASA Glenn Research Center, NASA/CR-2003-212529, Report ARL-CR-0531, USA, 2003.

[51] Sang Yup Jang, Seung Hoon Nahm, Chang Min Sui, Jung Soo Ha and Jung Soo Ha, "The Comparison of Fatigue crack Growth Behaviour for Long Term use and Heat treated 1Cr-0.5Mo Steel Under various Load Frequencies and Temperature," *International Journal of Modern Physics B,* vol. 19, no. 8 & 9, pp. 1640-1645, 2003.

[52] Heui-Huang Lee, Finite Element Simulations with ANSYS Workbench 15: Theory, Applications, Case Studies, USA: SDC Publications, 2014.

[53] S.S.Manson and G.R.Halford, Fatigue and Durability of Structural Materials, United State of America: ASM International, 2006.

[54] T.L Anderson, Fracture Mechanics: Fundamentals and Applications, USA: CRC Taylor & Francis, 2005.

[55] T.L.Anderson, "Damage Tolerance Methodology," in *Fracture Mechanics: Fundamentals and Applications*, USA, CRC Press, Taylor and Francis Group, 2005, pp. 501-503.